Network Dynamics and Learning

Homework III

Aljosevic Ismail s337769 Parovic Ana s344174

Academic Year 2025–2026

Introduction

This report presents the solutions to Homework III, which focuses on epidemic processes and game theory. The first part studies epidemic spreading using a simplified SIR model on different network topologies, including regular and random graphs, and analyzes the effects of vaccination and network structure on disease propagation. The second part addresses network games, where agents with coordination and anti-coordination objectives interact on a complete graph, and investigates the resulting Nash equilibria and learning dynamics under best response and noisy best response rules. All tasks were implemented in Python.

Exercise 1

In this exercise, we study the effects of the 2009 H1N1 pandemic in Sweden. In the first part, we simulate disease propagation using the simplified SIR epidemic model on both given and randomly generated graphs. Next, we analyze the impact of vaccination on the spread of the disease. In the final part, we estimate the characteristics of the network structure and report the resulting disease dynamics parameters.

1.1 Epidemic on a known graph

The epidemic is first simulated on a symmetric k-regular undirected graph, where each node is connected to the k nodes whose indices are closest to its own, computed modulo n.

The simulation follows a simplified SIR epidemic model. At each discrete time step $t = 1, 2, \ldots$, every node i can be in one of three possible states,

$$X_i(t) \in \{S, I, R\},$$

where S denotes a susceptible state, I denotes an infected state, and R denotes a recovered state.

The epidemic dynamics are governed by the following transition probabilities. A susceptible node becomes infected with probability

$$P\big(X_i(t+1) = I \,\big|\, X_i(t) = S,\ \sum_{j \in V} W_{ij}\, \delta^I_{X_j(t)} = m\big) = 1 - (1-\beta)^m,$$

where m is the number of infected neighbors of node i at time t.

An infected node recovers with probability

$$P\big(X_i(t+1) = R \,\big|\, X_i(t) = I\big) = \rho.$$

Let $\beta \in [0,1]$ denote the probability that an infection is transmitted from an infected node to a susceptible neighbor during a single time step. If a susceptible node i has m infected neighbors at time t, then the probability that node i is not infected by any of its infected neighbors during that time step is

$$(1-\beta)^m.$$

Consequently, the probability that node i becomes infected during that time step is

$$1 - (1-\beta)^m.$$

Furthermore, let $\rho \in [0,1]$ denote the probability that an infected node recovers during a single time step.

The matrix W_{ij} is the adjacency matrix of the network, and $\delta^I_{X_j(t)}$ is an indicator function that equals 1 if node j is infected at time t and 0 otherwise. Therefore,

$$\sum_{j \in V} W_{ij}\, \delta^I_{X_j(t)}$$

gives the number of infected neighbors of node i at time t.

Overall, the epidemic evolves dynamically over time. At each time step, transition probabilities are updated based on the current number of infected neighbors for each node. Susceptible nodes become infected according to these probabilities, while infected nodes recover randomly according to the recovery probability ρ.

In particular, we simulate the epidemic on a symmetric graph with parameters $k = 4$ and $|V| = 500$, using $\beta = 0.3$ and $\rho = 0.7$. One unit of time corresponds to one week, and the epidemic evolves over a period of 15 weeks. Initially, 10 nodes are selected uniformly at random from the node set V and set to the infected state. The simulation is repeated $N = 100$ times. The results, shown in the figure 1, report the average number of newly infected nodes at each week over all simulation runs.

We observe that the average number of newly infected individuals per week decreases monotonically over time, indicating that the epidemic reaches its peak at the beginning of the simulation and then gradually dies out.

To further analyze this behavior, we examine the influence of node degree on the average number of newly infected per week. The results for different values of k are shown in Figure 2.

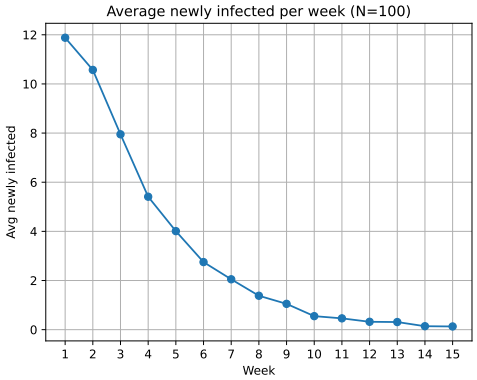

Figure 1: Average number of newly infected individuals per week on the symmetric k-regular graph.

When the node degree is increased to $k = 8$, the epidemic no longer goes extinct but persists over time with a moderate and sustained number of new infections. In contrast, for $k = 16$, the epidemic spreads very rapidly, producing a strong early peak and then quickly exhausting the susceptible population, which leads to a rapid decline in new infections.

The average numbers of susceptible, infected, and recovered individuals over time are shown in Figure 3.

The plots reveal several notable behaviors. In particular, the number of infected individuals closely follows the number of newly infected individuals shown in Figure 2. Once the number of newly infected individuals begins to decrease, the total number of infected individuals also declines almost simultaneously. This observation indicates that there is no significant accumulation of infected individuals over time. Most individuals who become infected in a given week recover within the same or the following week, suggesting that the average duration of the infection is approximately one week. As a result, the epidemic dynamics are primarily driven by the number of new infections occurring each week, rather than by a long-term persistence of infected individuals in the population.

1.2 Generation of a random graph

In this part, the graph is generated using the preferential attachment model. The construction of the model is described as follows.

At time $t = 0$, we start from an initial undirected graph G_0. At each subsequent time step t, a new graph G_t is obtained by adding one new node to the existing graph G_{t-1}. The newly added node is then connected to a subset of existing nodes according to a stochastic rule.

Under the preferential attachment mechanism, at every time step $t \geq 2$, the

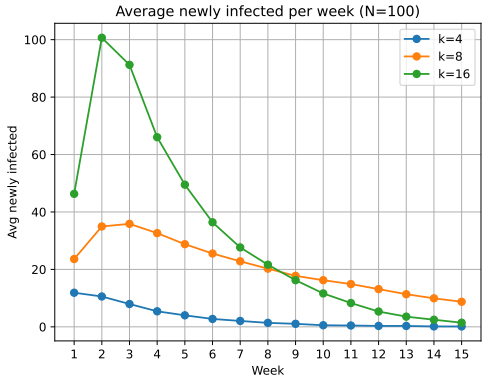

Figure 2: Epidemic evolution for different values of the node degree k.

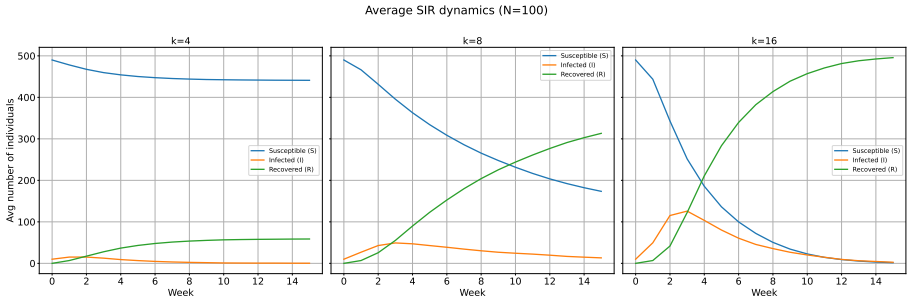

Figure 3: Average numbers of susceptible, infected, and recovered individuals over time for different values of k.

newly added node is assigned a fixed degree

$$w_{n_t}(t) = c = \frac{k}{2}.$$

That is, the new node introduces c undirected edges to the graph G_{t-1}. The existing nodes to which the new node connects are chosen probabilistically, with higher-degree nodes being more likely to receive new connections.

More precisely, let n_t denote the node added at time t. The probability that an edge is formed between n_t and an existing node $i \in \mathcal{V}_{t-1}$ is given by

$$\mathbb{P}(W_{n_t,i}(t) = W_{i,n_t}(t) = 1 \mid \mathcal{G}_{t-1}) = \frac{w_i(t-1)}{\sum_{j\in\mathcal{V}_{t-1}} w_j(t-1)}, \qquad i \in \mathcal{V}_{t-1}.$$

If k is an odd number, then $c = k/2$ is not an integer. Nevertheless, it is still possible to achieve an average node degree of k as the network grows. This can be accomplished by alternating between adding $\lfloor k/2 \rfloor$ and $\lceil k/2 \rceil$ edges when

introducing new nodes, so that the average number of added edges converges to $k/2$.

1.3 Simulating a pandemic without vaccination

In this part, we use a graph generated by the preferential attachment model with parameters $k = 6$ and $|V| = 500$, and epidemic parameters $\beta = 0.3$ and $\rho = 0.7$. The simulation is again performed over a period of 15 weeks. Results for the average number of newly infected individuals and the total numbers of susceptible, infected, and recovered individuals are shown in Figures 4 and 5, respectively.

The results obtained on the preferential attachment network show a rapid and intense spreading process. The number of newly infected individuals exhibits a strong early peak, indicating fast transmission driven by highly connected nodes. After the early peak, the number of infected and newly infected individuals quickly declines, suggesting that the epidemic dies out once the highly connected nodes are exhausted (hub nodes).

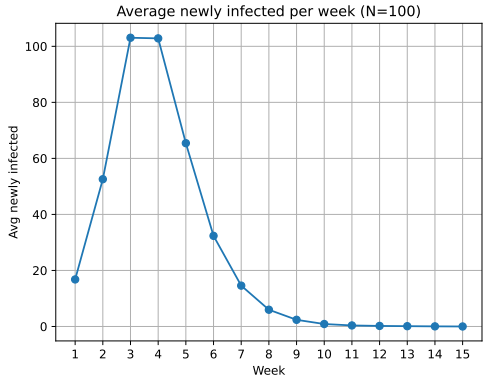

Figure 4: Average number of newly infected individuals per week on the preferential attachment graph.

1.4 Simulating a pandemic with vaccination

In this part, we introduce vaccination as a control measure to slow down the epidemic spread. In particular, a fraction of the population is vaccinated each week. Once an individual is vaccinated, they cannot become infected, and the vaccination is assumed to take effect immediately.

The vaccination distribution is given by

$$\text{Vacc}(t) = [0, 5, 15, 25, 35, 45, 55, 60, 60, 60, 60, 60, 60, 60, 60],$$

which represents the cumulative percentage of vaccinated individuals over time.

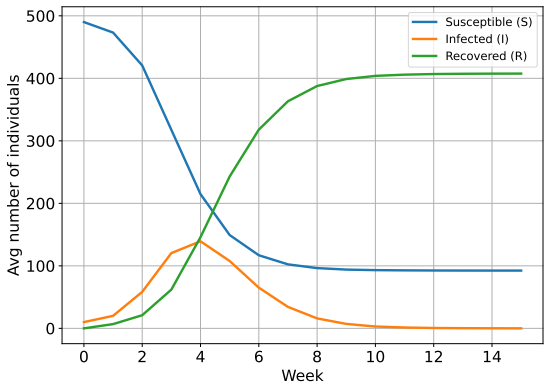

Figure 5: Average total numbers of susceptible, infected, and recovered individuals over time on the preferential attachment graph.

Each week, individuals to be vaccinated are selected uniformly at random from the population that has not yet been vaccinated. This selection includes susceptible, infected, and recovered individuals. This assumption reflects the fact that individuals may not be aware of whether they are infected or have already recovered from the H1N1 virus.

According to the given vaccination distribution, we compute the exact number of individuals to be vaccinated each week. Once vaccinated, an individual is assumed to neither become infected nor infect others, regardless of their state prior to vaccination. The effect of vaccination is immediate; therefore, individuals vaccinated in a given week cannot be infected during that same week. Moreover, individuals who are infected at the time of vaccination are assumed to recover immediately.

We perform the simulation using the same network and epidemic parameters as in the previous case. The results for the average number of newly infected individuals and the average total numbers of susceptible, infected, and recovered individuals are shown in Figures 6 and 7, respectively.

From these results, we observe that vaccination significantly reduces the magnitude of the epidemic and shortens its duration by approximately one week. The peak number of infected individuals is lower in the vaccinated scenario, and the epidemic ends earlier compared to the case without vaccination. Furthermore, the total number of infected individuals is reduced by more than 100 due to preventive vaccination. These results demonstrate that vaccination is an effective strategy for limiting disease spread and reducing the overall number of infections.

1.5 The H1N1 pandemic in Sweden, 2009

In this part, we use the models and methods developed in the previous sections to estimate the social network structure of the Swedish population and the

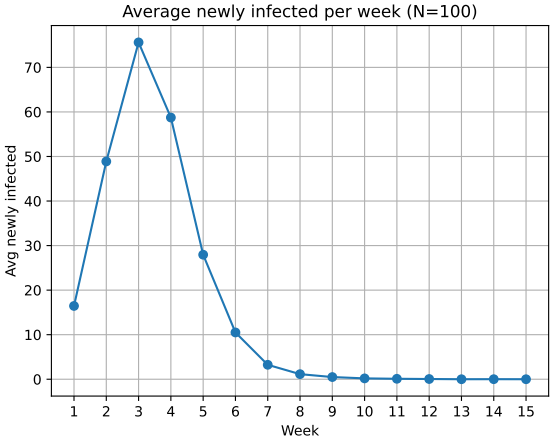

Figure 6: Average number of newly infected individuals per week with vaccination.

disease-spreading parameters during the 2009 H1N1 pandemic.

During the fall of 2009, approximately 1.5 million people out of a total population of about 9 million were infected with H1N1, and around 60% of the population received vaccination. We simulate the pandemic over the period from week 42 of 2009 to week 5 of 2010. During this time, the cumulative fraction of the population that had received vaccination is given by

$$\text{Vacc}(t) = [5, 9, 16, 24, 32, 40, 47, 54, 59, 60, 60, 60, 60, 60, 60].$$

To reduce computational complexity, the population size is scaled down by a factor of 10^4. Ground truth data describing the real epidemic evolution are available. The objective of this part is to determine the set of model parameters that best reproduces the observed epidemic behavior.

Gradient-Based Algorithm for Parameter Search

In this part, we use a provided gradient-based search algorithm over the parameter space (k, β, ρ) to identify the set of parameters that best reproduces the observed dynamics of the real H1N1 pandemic.

Initialization We start from an initial guess of the parameters and predefined step sizes:

$$k_0 = 10, \quad \beta_0 = 0.3, \quad \rho_0 = 0.6,$$
$$\Delta k = 1, \quad \Delta\beta = 0.1, \quad \Delta\rho = 0.1.$$

However, during the parameter search, we varied the step sizes Δk, $\Delta\beta$, and $\Delta\rho$. We started with larger step sizes and progressively divided them by 2 when no further improvement was observed.

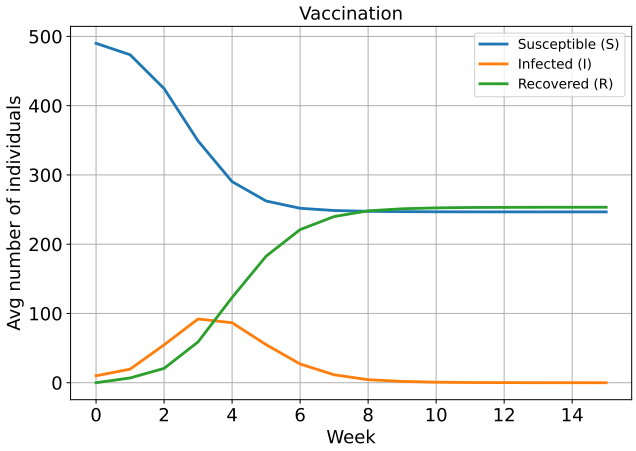

Figure 7: Average total numbers of susceptible, infected, and recovered individuals over time with vaccination.

Parameter Search For each combination of parameters

$$k \in \{k_0 - \Delta k,\, k_0,\, k_0 + \Delta k\},$$

$$\beta \in \{\beta_0 - \Delta\beta,\, \beta_0,\, \beta_0 + \Delta\beta\},$$

$$\rho \in \{\rho_0 - \Delta\rho,\, \rho_0,\, \rho_0 + \Delta\rho\},$$

the following steps are performed:

1. A random graph $G = (V, E)$ is generated using the preferential attachment model described in Section 1.1, with $|V| = 934$ nodes and an average degree equal to k.

2. Starting from week 42, the pandemic is simulated for 15 weeks on graph G using the vaccination model described in Section 1.3. The simulation is repeated $N = 10$ times, and the average number of newly infected individuals per week, denoted by $I(t)$, is computed.

3. The root-mean-square error (RMSE) between the simulated data and the real pandemic data is computed as

$$\text{RMSE} = \sqrt{\frac{1}{15}\sum_{t=1}^{15}\left(I(t) - I_0(t)\right)^2},$$

where $I(t)$ is the simulated average number of newly infected individuals in week t, and $I_0(t)$ denotes the corresponding value from the real data.

Update Rule The parameter set (k_0, β_0, ρ_0) is updated to the combination that yields the minimum RMSE. The algorithm terminates when the updated parameters coincide with those from the previous iteration.

Results

The smallest RMSE is obtained for the following set of parameters:

$$k = 8, \quad \beta = 0.1875, \quad \rho = 0.625.$$

The results obtained using this parameter set are shown in Figures 8 and 9.

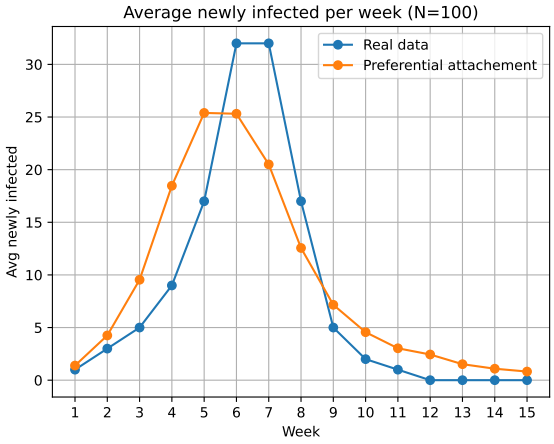

Figure 8: Comparison between the simulated and real average number of newly infected individuals per week.

Overall, the model captures the general epidemic trend well. However, it exhibits a slightly faster initial spread, an earlier and lower peak, and a slower decay compared to the real epidemic data.

1.6 Challenge (Optional) – Small-World Network

This model is motivated by the empirical observation that many real-world networks exhibit a small diameter and a high level of clustering.

The preferential attachment model tends to generate a small number of highly connected hub nodes, which may not be the most intuitive representation of epidemic spreading. In practice, diseases often propagate through multiple small, densely connected groups rather than through a few dominant hubs. Individuals within such groups interact frequently, while only a limited number of connections link different groups together.

A simple illustrative example is a classroom of students, which forms a small, highly connected group. If one student becomes infected, the disease

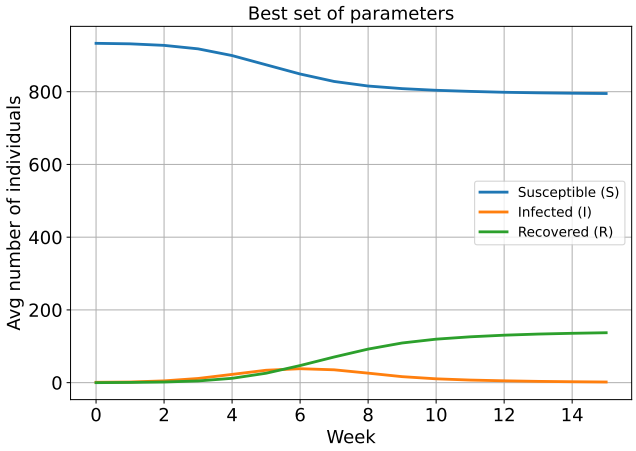

Figure 9: Average total numbers of susceptible, infected, and recovered individuals obtained with the estimated parameters.

can spread rapidly within the classroom. These students are also connected to their families, which form additional tightly connected groups. Family members, in turn, interact closely with colleagues in the workplace, creating further clusters. Through these inter-group connections, the disease can spread across different social contexts and eventually propagate throughout the population.

In fact, the symmetric k-regular graph introduced in Section 1.1 represents the basic structure of a small-world network. To better capture small-world properties, we extend this model by introducing a number of random long-range connections between nodes. The obtained results are shown in Figure 10.

The proposed small-world network produces results that are broadly similar to those obtained with the preferential attachment model. Notably, both models tend to overestimate the number of infected individuals during the first five weeks and after the epidemic peak, while simultaneously underestimating the peak magnitude of the pandemic. This suggests that the models struggle to balance early growth, peak intensity, and post-peak decay.

A possible and intuitive approach to improve the model performance is to modify the loss function used during parameter estimation. In particular, we experiment with replacing the standard RMSE by a weighted RMSE, allowing different phases of the epidemic to be emphasized differently.

The **Weighted Root Mean Squared Error (WRMSE)** is an error metric that assigns different weights to individual observations, allowing certain time points to have a greater influence on the overall error. It is defined as

$$\text{WRMSE} = \sqrt{\frac{\sum_{i=1}^{n} w_i \left(y_i - \hat{y}_i\right)^2}{\sum_{i=1}^{n} w_i}},$$

where y_i denotes the true values, $\hat{y}_i$ the predicted values, and w_i the weights

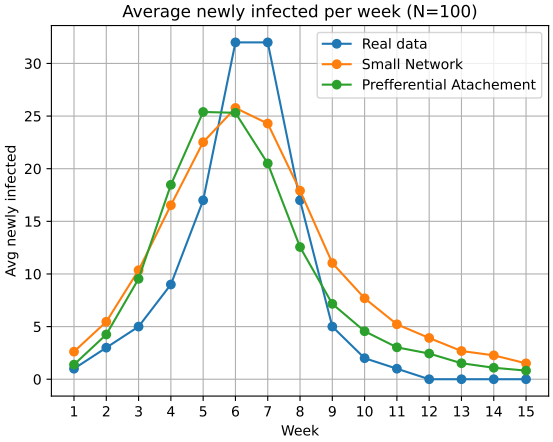

Figure 10: Comparison of epidemic evolution across different network models.

representing the relative importance of each observation.

In our experiment, we used weights proportional to the real number of newly infected individuals $w_t = I_0(t) + 1$. This choice emphasizes the peak weeks (where $I_0(t)$ is largest), while the $+1$ term ensures nonzero weight also in weeks with $I_0(t) = 0$.

Compared to the RMSE-based optimization, the use of WRMSE improves the agreement with real data primarily in the peak region of the epidemic. In particular, both the timing and the magnitude of the peak of newly infected individuals are more accurately captured, while the accuracy in the early growth phase and the late decay phase remains almost unchanged.

In epidemic modeling, accurately identifying the peak of the epidemic is often more important than minimizing errors uniformly over time, as reliable peak estimation enables better preparedness of healthcare systems and more effective allocation of resources.

Randomized Hyperparameter Tuning and Bayesian Search

Finally, we note that the gradient-based parameter search used in this work can be relatively slow, since it requires running multiple epidemic simulations for many parameter combinations. As an alternative, more efficient hyperparameter optimization methods could be explored, such as *random search* and *Bayesian optimization*. These approaches are often able to identify good parameter settings using fewer evaluations, and could therefore reduce computational cost while potentially improving the fit to the real epidemic data.

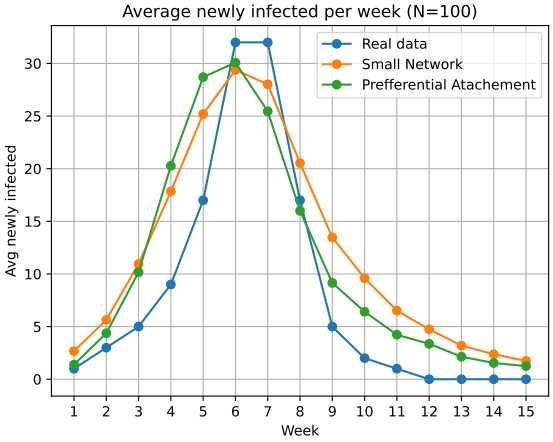

Figure 11: Comparison of epidemic evolution across different network models with WRMSE.

Exercise 2

The second part focuses on the Network Games and Dynamics. We consider a game defined by $(V, A, \{u_i\})$, where the set of players is $V = \{1, \ldots, n\}$ and the action set is $A = \{-1, +1\}$. The players are divided into two classes $V_1 = \{1, \ldots, n_1\}, V_2 = \{n_1 + 1, \ldots, n\}$, and the utility functions are given by

$$u_i(x_i, x_{-i}) = \begin{cases} \frac{1}{2} \sum_{j \neq i} |x_i + x_j|, & \text{if } i \in V_1, \\ \frac{1}{2} \sum_{j \neq i} |x_i - x_j|, & \text{if } i \in V_2. \end{cases}$$

Players in V_1 have the utility function of a network coordination game, while players in V_2 have the utility function of a network anti-coordination game. The objective is to determine the Nash equilibria of the game when $n = 3$ for the following cases:

$$|V_1| = n_1 \in \{3, 2, 1, 0\}.$$

The interaction structure of the game is represented by a complete graph, meaning that every player directly interacts with every other player and therefore influences, and is influenced by, all other players.

2.1 Nash equilibria for $n_1 = 3$ and $n_1 = 0$

We first consider the case $n_1 = 3$, where all players belong to the set V_1 and therefore follow the utility function of a coordination game. In this setting, each

player maximizes its utility by choosing the same action as the majority of the other players. Since the interaction network is represented with complete graph, this game corresponds to a majority coordination game, and thus the only Nash equilibria are the two consensus configurations $(+1, +1, +1)$, $(-1, -1, -1)$. In both configurations, no player has an incentive to deviate unilaterally, since any deviation would strictly decrease its utility.

In the case $n_1 = 0$, all players belong to the set V_2 and therefore follow the utility function of an anti-coordination game. In this setting, each player prefers to choose an action different from the actions chosen by the other players. This game can be interpreted as a minority game on a complete graph. The minority game on a complete graph with odd number of nodes admits multiple Nash equilibria. These equilibria can be divided into two symmetric classes: in one class, $\frac{n-1}{2}$ players choose the first strategy and $\frac{n+1}{2}$ players choose the second strategy, while in the other class the roles of the two strategies are exchanged. It is important to state that none of these equilbria are strict.

We confirmed these results using numerical simulations, where we systematically evaluated all possible action configurations and verified whether each configuration satisfies the Nash equilibrium condition by computing unilateral deviations in individual utilities. The results are illustrated in Figures 12 and 13. In these figures, the label on each node indicates the group to which the player belongs, while the node color represents the chosen action.

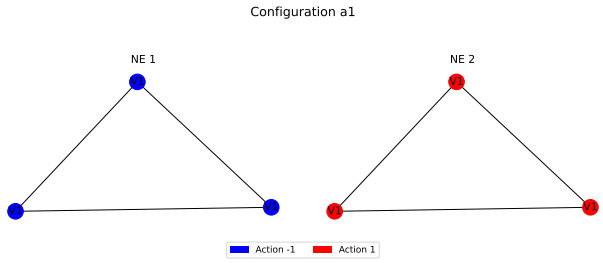

Figure 12: Nash equilibria for the case $|V_1| = n$ and $|V_2| = 0$.

2.2 Nash equilibria for $n_1 = 2$ and $n_1 = 1$

In both of these cases, the game simultaneously exhibits features of both majority and minority games. In this setting, some nodes have the utility function of a majority game, while others have the utility function of a minority game.

In general, determining the existence and structure of Nash equilibria for this class of heterogeneous network games is a difficult problem. For this reason, we adopt a numerical approach in order to identify the configurations corresponding to Nash equilibria. The obtained results are summarized below and illustrated in Figures 14 and Figures 15.

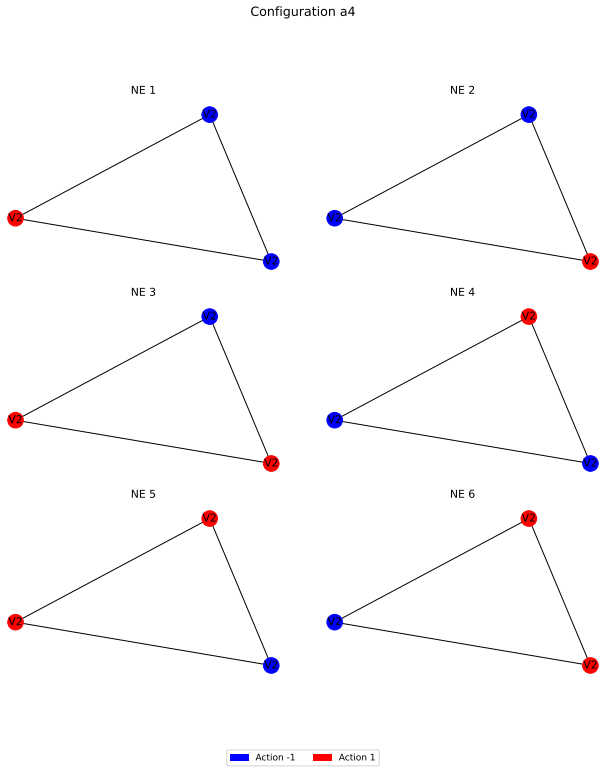

Figure 13: Nash equilibria for the case $|V_1| = 0$ and $|V_2| = n$.

- Nash equilibria for the case $n_1 = 2$:

$$(-1, -1, 1),\ (1, 1, -1)$$

- Nash equilibria for the case $n_1 = 1$:

$$(-1, -1, 1),\ (-1, 1, -1),\ (-1, 1, 1),\ (1, -1, -1),\ (1, -1, 1),\ (1, 1, -1)$$

For the case $n_1 = 2$ (shown in Figure 14), two players aim to match the actions of the other players, while the third player adopts an opposite strategy. The Nash equilibria correspond to configurations in which the two players in group V_1 choose the same action, and the player in group V_2 chooses the opposite action.

For the case $n_1 = 1$ (shown in Figure 15), two players follow an anti-coordination principle, while the third player copies their actions. The Nash equilibria correspond to configurations in which the player in group V_1 copies the action of one of its neighbors, while the remaining player in group V_2 chooses the opposite action. All symmetric configurations are equilibria; thus none of them are strict.

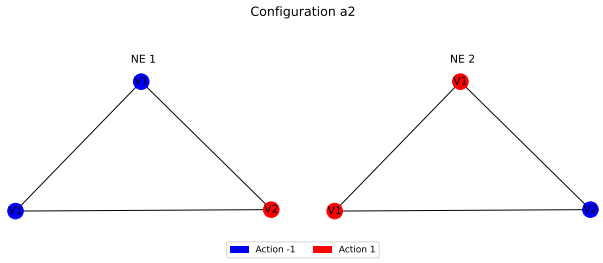

Figure 14: Nash equilibria for the case $|V_1| = 2$ and $|V_2| = 1$.

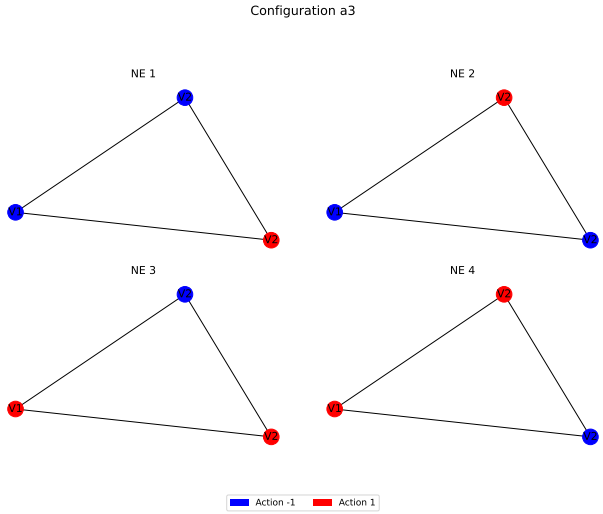

Figure 15: Nash equilibria for the case $|V_1| = 1$ and $|V_2| = 2$.

2.3 Discrete-Time Asynchronous Best Response Dynamics and Noisy Best Response Dynamics

The **discrete-time asynchronous Best Response (BR) dynamics** is a Markov chain $X(t)$ with state space $\mathcal{X} = \mathcal{A}^{\mathcal{V}}$, which coincides with the set of all action profiles of the game. At each time step t, a player $i \in \mathcal{V}$ is selected uniformly at random and updates her action by choosing a best response uniformly at random from the set $B_i(X_{-i}(t))$, where

$$B_i(X_{-i}(t)) := \arg\max_{a_i \in \mathcal{A}_i} u_i(a_i, X_{-i}(t)).$$

Formally, the update rule is given by

$$\mathbb{P}(X_i(t+1) = a_i \mid X(t)) = \begin{cases} \dfrac{1}{|B_i(X_{-i}(t))|}, & a_i \in B_i(X_{-i}(t)), \\ 0, & \text{otherwise}, \end{cases}$$

while $X_j(t+1) = X_j(t)$ for all $j \neq i$.

In other words, a player changes her action only if doing so strictly improves her utility or leaves it unchanged. As a consequence, this dynamics may become trapped in Nash equilibria that are not global maximizers of the potential function, if such equilibria exist.

The **discrete-time noisy best response (NBR) dynamics** is also defined as a Markov chain $X(t)$ on the state space $\mathcal{X} = \mathcal{A}^{\mathcal{V}}$. At each time step t, one player $i \in \mathcal{V}$ is selected uniformly at random and updates her action according to the logit choice rule

$$\mathbb{P}(X_i(t+1) = a_i \mid X(t)) = \frac{e^{\eta\, u_i(a_i, X_{-i}(t))}}{\sum_{a_i' \in \mathcal{A}_i} e^{\eta\, u_i(a_i', X_{-i}(t))}},$$

while the actions of all other players remain unchanged. The parameter $\eta > 0$ represents the inverse noise level.

If the underlying game is a potential game with potential function $\Phi\colon \mathcal{X} \to \mathbb{R}$, the NBR dynamics is irreducible and admits a unique invariant distribution π whose support is the entire configuration space $\mathcal{X}$. This invariant distribution is given by the Gibbs distribution

$$\pi(x) = \frac{e^{\eta\Phi(x)}}{Z_\eta}, \qquad Z_\eta = \sum_{y \in \mathcal{X}} e^{\eta\Phi(y)}.$$

In the vanishing noise limit $\eta \to \infty$, the invariant distribution concentrates on the set of global maximizers of the potential function Φ. For finite values of η, every configuration is visited with positive probability.

2.3.1 Majority game : $n_1 = 3$

We consider the Majority Game with $n_1 = 3$ players. The action space is

$$x \in \{-1, +1\}^3.$$

We study the limit

$$\lim_{t \to +\infty} \mathbb{P}\big(X(t) = x \mid X(0) = (+1, -1, +1)\big).$$

The game admits exactly two Nash equilibria,

$$(+1, +1, +1) \quad \text{and} \quad (-1, -1, -1),$$

which correspond to consensus configurations (see Figure 12). Both equilibria are global maximizers of the potential function. Under BR dynamics, these states are absorbing.

The BR dynamics induces a non-irreducible Markov chain and therefore does not admit a unique invariant distribution. As a consequence, the limiting distribution depends on the initial condition.

Starting from

$$X(0) = (+1, -1, +1),$$

it is possible to reach both consensus equilibria. In particular, players currently choosing action $+1$ may switch to -1 without decreasing the potential, and similarly for players choosing -1. Hence, both absorbing states are reached with positive probability.

Therefore, there exist $p_+, p_- > 0$ with $p_+ + p_- = 1$ such that

$$\lim_{t\to+\infty} \mathbb{P}\big(X(t) = x \mid X(0) = (+1, -1, +1)\big) = \begin{cases} p_+, & x = (+1, +1, +1), \\ p_-, & x = (-1, -1, -1), \\ 0, & \text{otherwise.} \end{cases}$$

All non-consensus configurations are transient states, which explains why their limiting probabilities are equal to zero.

The values of p_+ and p_- are obtained by computing the hitting probabilities of the two absorbing states, either by simulation or by solving a linear system using the transition matrix P. The resulting values are

$$p_+ = \frac{2}{3}, \qquad p_- = \frac{1}{3}.$$

In the case of NBR dynamics, the induced Markov chain is reversible and irreducible, and therefore admits a unique stationary distribution, independently of the initial condition. This stationary distribution can be obtained by solving the stationary equation in Gibbs form.

In our setting, the value $\eta = 10$ corresponds to the vanishing-noise regime. The resulting stationary distributions is given by

$$\pi = \begin{bmatrix} 0.50 & 0.00 & 0.00 & 0.00 & 0.00 & 0.00 & 0.00 & 0.50 \end{bmatrix}$$

where the first element corresponds to the state $(-1, -1, -1)$, and the last element corresponds to the state $(1, 1, 1)$. This is according to the statements that Gibbs distribution in the vanishing noise limits converges to a uniform probability over the set of configurations that are the global maximizers of the potential function,

The obtained results obtained differ from those obtained under BR dynamics. For most of the time, NBR behaves similarly to BR. However, when observed over sufficiently long time horizons, the process spends asymptotically a fraction $1/2$ of the time in the configuration with all $+1$ and a fraction $1/2$ of the time in the configuration with all -1, independently of the initial condition. Although NBR leaves the set of global maximizers of the potential function with very small probability, once such a transition occurs, the process typically remains for a long time in the newly visited state before another rare transition takes place.

We also verified this behavior empirically. Since sufficiently large values of η theoretically yield the same invariant distribution, we perform empirical simulations using $\eta = 5$. This choice allows us to significantly reduce the computational

time required for the simulations. Indeed, for large values of η, transitions away from the global maximizers of the potential function are very rare, and therefore extremely long simulation runs would be required to observe such transitions.

2.3.2 Minority game: $n_1 = 0$

In the Minority game, Nash equilibria exist, but none of them are strict (see Figure 13). In every equilibrium configuration, there are players who are indifferent between their available actions. Consequently, under BR dynamics, transitions between equilibrium configurations are always possible. As a result, all equilibria belong to a single aperiodic connected sink component.

Although the Markov chain induced by BR dynamics is not irreducible, the presence of a single closed and aperiodic component implies the existence of a unique stationary distribution supported on that component. All other states are transient, and the chain converges to this stationary distribution independently of the initial state.

The stationary distribution therefore satisfies

$$\lim_{t\to+\infty} \mathbb{P}\big(X(t) = x \mid X(0) = (+1,-1,+1)\big) = \pi(x),$$

where

$$\pi(i) = \begin{cases} \pi_C(i), & i \in C, \\ 0, & i \notin C, \end{cases}$$

and C denotes the sink component.

The stationary distribution obtained under BR dynamics is

$$\pi = \begin{bmatrix} 0.00 & 0.17 & 0.17 & 0.16 & 0.17 & 0.17 & 0.17 & 0.00 \end{bmatrix}.$$

In the case of NBR dynamics, we obtain the identical stationary distribution by solving the stationary equation in Gibbs form.

Given the initial condition $X(0) = (+1,-1,+1)$, if the equilibrium configurations were only local maximizers of the potential function, then under BR dynamics the process would become trapped in one of these equilibria. In contrast, under NBR in vanishing noise limit dynamics, although escapes from such local maxima are rare, they remain possible due to the reversibility and irreducibility of the induced Markov chain.